ACS Photonics

pubs.acs.org/journal/apchd5

Article

Toward Stand-Alone Alkali-Based Mid-Infrared Frequency References

Yoel Sebbag, Roy Zektzer, Yefim Barash, and Uriel Levy*

Cite This: *ACS Photonics* 2020, 7, 1508−1514

Read Online

ACCESS | Metrics & More | Article Recommendations | Supporting Information

ABSTRACT: Highly accurate and precise spectroscopy in the mid-infrared (MIR) spectral region is a versatile tool that finds great interest in fundamental scientific research as well as in mitigating myriad applications in diverse fields. A major driving force for the rapidly increasing interest in MIR spectroscopy is the emergence of quantum cascade lasers (QCLs). Yet, as of today, such QCLs are still experiencing significant free-running frequency fluctuations which makes their frequency stabilization challenging. Here, we propose and experimentally demonstrate a method enabling development of frequency standards in the MIR, based on high excited stats of alkali vapors. The technique is based on the generation of a Doppler-free gain spectrum in the MIR by copropagating two stabilized pump near-infrared (NIR) lasers. Using this technique, the frequency of a distributed feedback (DFB) QCL at 5.23 μm is stabilized to the corresponding $6^2P_{3/2}-5^2D_{5/2}$ transition of rubidium (Rb) vapors, showing a substantial stability improvement compared to the free-running operation. Stabilization to an atomic MIR transition can be implemented in a rather simple scheme, with diverse applications. For example, the approach may enable the development of highly accurate self-calibrated optical spectrometers and can also be used for direct stabilization of MIR frequency combs.

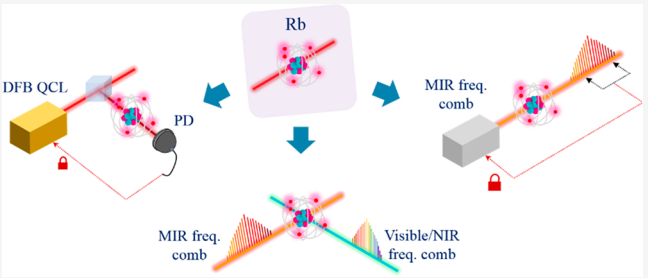

KEYWORDS: *metrology, mid-infrared spectroscopy, quantum cascade lasers, atoms*

Spectroscopy in the so-called "molecular fingerprint" spectral region (3−20 μm) yields critical information on material structure for physical, chemical, and biological sciences. High-precision atomic and molecular spectroscopy is extensively used in fundamental research as well as in practical applications. These two domains have generally different requirements. Researchwise, ultrahigh precision frequency standards can reach a fractional stability of 10^{-18},[1−3] and they are generally used to test fundamental symmetries such as parity and time reversal[4−7] or to measure the absolute values of fundamental constants and their potential variation in time.[8−10] Looking more into applications, compact atomic frequency standards, aimed at commercial and industrial market requires a typical fractional frequency stability in the range of 10^{-10} to 10^{-13}.[11−15] The MIR spectral range is also of great interest for many applications such as gas detection,[16] cold molecules manipulations,[17] and molecular frequency metrology,[18] to name a few. The wide expansion of this field can be attributed to the development of the QCLs, which cover a wide spectral region in the MIR. However, their significant free-running frequency fluctuations limits their applications in high-precision spectroscopy. This calls for an immediate remedy in the form of frequency stabilization.

Frequency stabilization of a QCL to a molecular rovibrational transition in the MIR presents limitations regarding their frequency reproducibility and accuracy.[5,19−27] To circumvent this obstacle, efforts have been made to stabilize QCLs to a stable NIR laser. By doing so, the stability of the NIR source was transferred all the way to the MIR spectral region via a stabilized MIR frequency comb.[19,21,24,28−31] This approach allowed to achieve a high relative stability and accuracy of about 2×10^{-15}.

An alternative for achieving high precision molecular spectroscopy is to use a calibrated MIR Fourier transform infrared (FTIR) spectrometer, which is generally limited in its accuracy by the precision of the calibration laser. For example, in the telecom regime, optical spectrometers can be self-calibrated by NIR lasers, which are typically stabilized to acetylene transitions.[32]

As it turns out, many alkali atoms, which are frequently used in metrology, atomic clock, and NIR frequency references,[33] also present less commonly used, yet accessible, MIR transitions[34−36] that can be utilized as frequency references. In this work, we propose a method to generate a MIR Doppler-

Received: February 26, 2020
Published: May 19, 2020

https://dx.doi.org/10.1021/acsphotonics.0c00308
ACS Photonics 2020, 7, 1508−1514

free gain spectrum in the high excited states of alkali vapors and use it to experimentally demonstrate the frequency stabilization of a DFB QCL to the MIR transition of Rb atoms at 5.23 μm. In this scheme, the MIR transition is accessed via a two-colored pump beam, in a velocity selective copropagating configuration, also stabilized to Rb vapors, showing a significant improvement of the long-term stability of the laser, compared to free running laser operation. It should be emphasized that the presented technique can be applied to any similar MIR and even far IR transition of alkali vapors, for example, the $3^2D \rightarrow 4^2P$ transitions of Sodium vapors at about 9.09 μm, or the $6^2D \rightarrow 7^2P$ transitions of cesium vapors at 12.1 and 15.6 μm,[37] to name a few. Also, the presented technique can be used to directly stabilize a MIR frequency comb, for dual comb spectroscopy.

EXPERIMENTAL SETUP

The relevant energy levels of ^{85}Rb and a sketch of our experiment are presented in Figure 1. The upper $5^2D_{5/2}$ states

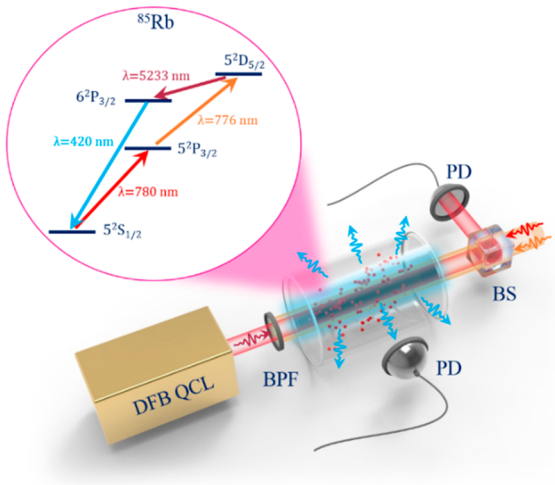

Figure 1. Simplified scheme of the experimental setup. BS: beam splitter, BPF: band-path filter, PD: photodetector. The inset presents the relevant atomic energy levels of ^{85}Rb.

of ^{85}Rb, and correspondingly, the $5^2D_{3/2}$ level of ^{87}Rb (see Supporting Information) can be easily accessed by a two-photon absorption and as such can be efficiently populated with relatively low power NIR laser diodes, at 780 and 776 nm, corresponding to the $5^2S_{1/2}-5^2P_{3/2}$ and the $5^2P_{3/2}-5^2D_{5/2}$ transitions, respectively. The pump lasers are copropagating and their frequency are locked to the $5^2S_{1/2}(F = 3)-5^2P_{3/2}(F = 4)$ and $5^2P_{3/2}(F = 4)-5^2D_{5/2}(F = 5)$ hyperfine cycling transitions of ^{85}Rb, using a wavelength modulation scheme.[38] Then, a MIR laser probes the $6^2P_{3/2}-5^2D_{5/2}$ transition.

Before interaction with the MIR laser, about 35% of the atomic population in the $5^2D_{5/2}$ level decays spontaneously to the $6^2P_{3/2}$ level,[39] and due to the difference in the radiative lifetime of these levels, population inversion can be achieved. Based on this effect, amplified spontaneous emission (ASE) and four-wave mixing at 5.23 μm was reported.[34−36] In our experiment, the pump power was kept relatively low in order to minimize these effects.

Common Rb reference cells, are made of either Pyrex or quartz and, thus, are not transparent in the MIR, above 3 μm. To tackle this obstacle, we have used a 10 cm long custom Rb cell with sapphire windows. The custom cell consists of a Pyrex tube with glass-to-metal adaptors at both ends. Two viewports with sapphire windows were attached and tightened to hold vacuum. The sapphire windows are as thin as about 1.57 mm thick to diminish absorption at the wavelength of 5 μm. The cell was connected to a high vacuum ($\sim 10^{-9}$ Torr) system and filled with natural Rb by distillation. Finally, the cell was sealed and disconnected from the distillation system with the end result of having a standalone and portable cell. The cell was heated to a temperature of about 60 °C, such that the density of the Rb was kept relatively low, at about 2×10^{11} cm^{-3} level, to minimize the dipole−dipole interactions, that could cause broadening and shift of the atomic levels.

In the experiment, two external cavity diode lasers (Toptica and Newfocus) were used for the 780 and 776 nm pumps. The beam diameter of the pump lasers was approximately 2 mm, and the optical power incident to custom cell was about 4 mW at 780 nm and 3.3 mW at 776 nm, corresponding to Rabi frequencies of about $\Omega_{780} \approx 2\pi \times 65$ MHz and $\Omega_{776} \approx 2\pi \times 17$ MHz, respectively. The MIR laser is the most sensitive part of the experiment. It consists of a custom-made room temperature DFB QCL (Thorlabs), designed to lase at a wavenumber around 1910.9 cm^{-1}, corresponding to the energy difference between the $6^2P_{3/2}$ and the $5^2D_{5/2}$ levels of Rb. It was operated at a temperature of 297 K and at current of 320 mA, delivering an output power of about 117 mW. However, only a small portion of about 7 μW were used for the spectroscopy measurements and the frequency stabilization in order to minimize power broadening. The beam diameter was also about 2 mm, and, given the absorption of the Sapphire window of about 30% and the Fresnel reflections, the actual probe power in the cell is estimated to be about 4.5 μW, corresponding to a Rabi frequency of $\Omega_{5233} \approx 2\pi \times 8$ MHz. Yet, An MCT detector cooled with 4 thermoelectric coolers (VIGO System) was used to detect the probe signal at 5.23 μm. As no isolator is available to us at this wavelength region, the experimental setup was built with extra care, in order to diminish the back-reflection that causing mode-hope and preventing us to achieve precise spectroscopy. The MIR wavelength-meter (Bristol Instruments, 671B-IR) is based on a Michelson interferometer, and it is self-calibrated to a standard, nonstabilized, He−Ne laser. The QCL is also stabilized to the MIR Rb transition by wavelength modulation technique.

RESULTS AND DISCUSSIONS

A. Generation of a MIR Doppler-Free Gain Spectrum.

Figure 2 presents the normalized spectroscopy measurements of the $6^2P_{3/2}-5^2D_{5/2}$ transition of ^{85}Rb. The MIR frequency was scanned by varying the current of the QCL as a function of time, while simultaneously, the actual frequency was measured with a commercially available MIR wavelength meter. When the MIR laser is on-resonance with one of the hyperfine transitions of Rb, it induces stimulated emission which is measured as a gain in the transmitted probe MIR signal, and, simultaneously, as enhanced blue fluorescence. The figure also presents fitting to a model. The different hyperfine transitions were identified by comparing the relative frequency separations between the measured peaks with the corresponding theoretical values (see Supporting Information) as well as comparing to the theoretical model.

The model is based on rate equations including 16 hyperfine levels of the $5^2S_{1/2}$, $5^2P_{3/2}$, $6^2P_{3/2}$, and $5^2D_{5/2}$ levels of ^{85}Rb. In this model the transition strength is calculated from quantum

https://dx.doi.org/10.1021/acsphotonics.0c00308
ACS Photonics 2020, 7, 1508−1514

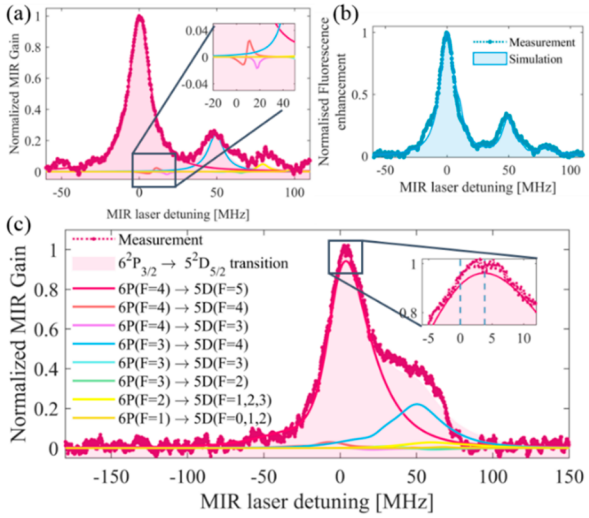

Figure 2. Spectroscopy of the $6^2P_{3/2}$−$5^2D_{5/2}$ transition of ^{85}Rb, for the case of copropagating pumps (a, b) and counter-propagating pumps (c). The graphs show the measured (dashed line) and simulated (solid lines) normalized MIR gain spectrum (a, c) and the normalized fluorescence enhancement in the blue at 420 nm (b). Each of the solid lines represents a specific hyperfine transition, as indicated in the legend of (c). The shaded area represents the superposition of all the solid lines. The inset in (a) shows a zoom on the contribution of the $6^2P_{3/2}(F = 4)$−$5^2D_{5/2}(F = 4)$ and $6^2P_{3/2}(F = 4)$−$5^2D_{5/2}(F = 3)$ hyperfine transitions. The inset in (c) shows a zoom of the main transition presenting a shift of about 3.85 MHz due to the overlapping of the broadened lines. These results were obtained using lock-in amplifier (Stanford RS830), while the intensity of the 780 nm laser was modulated with a chopper, for an increased signal-to-noise ratio.

mechanics model, and these transitions are allowed according to the selection rules. The effect of power broadening was added phenomenologically by substituting the natural line width of the transition, γ_0, by $\Gamma = \gamma_0 * \sqrt{1 + I/I_{sat}}$, where I is the intensity of the light and I_{sat} is the saturation intensity (see Supporting Information). The only free parameters of this model are the density of Rb, the intensity of the different lasers and their relative detuning form any transition. In Figure 2, the fitting to the experiment is obtained by assuming a pump power of 4 and 3 mW at 780 and 776 nm, respectively, and a probe power in the MIR of about 4 μW. Using these parameters, a relatively good agreement between the experiment and the theory was obtained.

In a velocity selective copropagating pumps configuration (Figure 2a,b), since the pump NIR lasers are locked to the $5^2S_{1/2}(F = 3)$−$5^2P_{3/2}(F = 4)$ and $5^2P_{3/2}(F = 4)$−$5^2D_{5/2}(F = 5)$ cycling transitions, only atoms with zero-velocity component in the propagation direction are on-resonance and can be pumped efficiently to the hyperfine $5^2D_{5/2}(F = 5)$ level. Thus, the main resonance at zero-detuning corresponds to the cycling transition $6^2P_{3/2}(F = 4)$−$5^2D_{5/2}(F = 5)$. This was confirmed by a simulation, which shows that the contribution of the other hyperfine transitions to this peak is negligible (inset in Figure 2a). The main resonance can be fitted to a Lorentzian with a line width of about 15.6 MHz, which is mainly due to power broadening, as compared with the 0.677 MHz natural lifetime of the $5^2D_{5/2}$ level.[39] Another resonance, with a smaller extinction and at a detuning of about 49.3 MHz, corresponds to the $6^2P_{3/2}(F = 3)$−$5^2D_{5/2}(F = 4)$ transition. It is shifted by about 0.64 MHz from its theoretical value (see Supporting Information). This can be explained by a two-photon absorption to the upper $5^2D_{5/2}(F = 4)$ level due to Doppler shift, which can be populated by a group of atoms with a velocity component, v of about v = 3.6 m/s in the propagation direction. The frequency shift, Δ_D, measured in the MIR transition is then $\Delta_D = (\omega/c)\cdot v/2\pi \approx 0.69$ MHz, where ω is the frequency of the MIR light and c is the speed of light in Rb.

Following the previous discussion, we have also investigated the case of counter-propagating pump lasers. In this scheme, the propagation direction of the 780 nm laser is flipped such that it is now counterpropagating with respect to a 776 nm pump laser, and copropagating with the MIR laser (see Supporting Information for experimental setup). Figure 2c presents the simulations and measurement of the MIR gain spectrum in the case of counterpropagating pumps. The simulation shows the relevant hyperfine transitions that construct the spectrum, also considering power broadening effect. The fitting parameters are similar to the case of copropagation pumps. In the counter-propagating configuration, the spectroscopy of Rb in the MIR shows wider resonances, with an effective line width of about 70 MHz, consisting of a main resonance having a line width of about 32 MHz and additional lines that are partially overlapping with it. This can be explained by the fact that since the wavelengths of the two pump lasers are close to each other, the Doppler shift experienced by atoms with a nonzero velocity component in the propagation direction cancels out, $(k_{780} - k_{776})\cdot v \approx 0$, such that their $5^2D_{5/2}(F = 5)$ level is efficiently populated. Thus, the MIR resonances are Doppler broadened, and the spectrum can be fitted with Voigt profiles. In this configuration, the $6^2P_{3/2}(F = 4)$−$5^2D_{5/2}(F = 5)$ hyperfine transition is efficiently excited, as well as other hyperfine transitions, due to power broadening (see Supporting Information). We have found that, because of this effect, the main resonance peak was shifted by about 3.85 MHz from its theoretical value (inset in Figure 2c). Thus, different groups of atoms, presenting a significant Doppler shift, can be efficiently populated in this scheme. This is in contrast to the copropagating velocity selective configuration, where a Doppler-free gain spectrum can be generated and no power-dependent shift was observed. Therefore, we conclude that the copropagating scheme is favorable over the counter propagating one for frequency referencing purposes.

B. Frequency Stabilization. We now describe the application of frequency stabilization based on the demonstrated Doppler-free MIR gain spectrum. Figure 3 summarizes the performance of the frequency stabilization scheme presented here. Figure 3a shows the overlapping Allan deviation, measured against our wavelength meter for the case of free-running laser operation and when the QCL is stabilized to the $6^2P_{3/2}(F = 4)$−$5^2D_{5/2}(F = 5)$ cycling transition of ^{85}Rb. The results show 30-fold improvement in the fractional frequency stability after about 2 min of integration time. The QCL frequency was stabilized to an accuracy of about 415 kHz, corresponding to a relative frequency of 7.3×10^{-9}. The measured fractional frequency instability of the MIR reference is $8.2 \times 10^{-8}/\tau^{1/2}$, presenting a typical behavior limited by white frequency noise,[40] which is attributed to our measuring tool.

The major noise sources are shown in the graph presenting the relative frequency measured by the closed-loop servo-electronic recorded in parallel to the reading of the wavelength

https://dx.doi.org/10.1021/acsphotonics.0c00308
ACS Photonics 2020, 7, 1508−1514

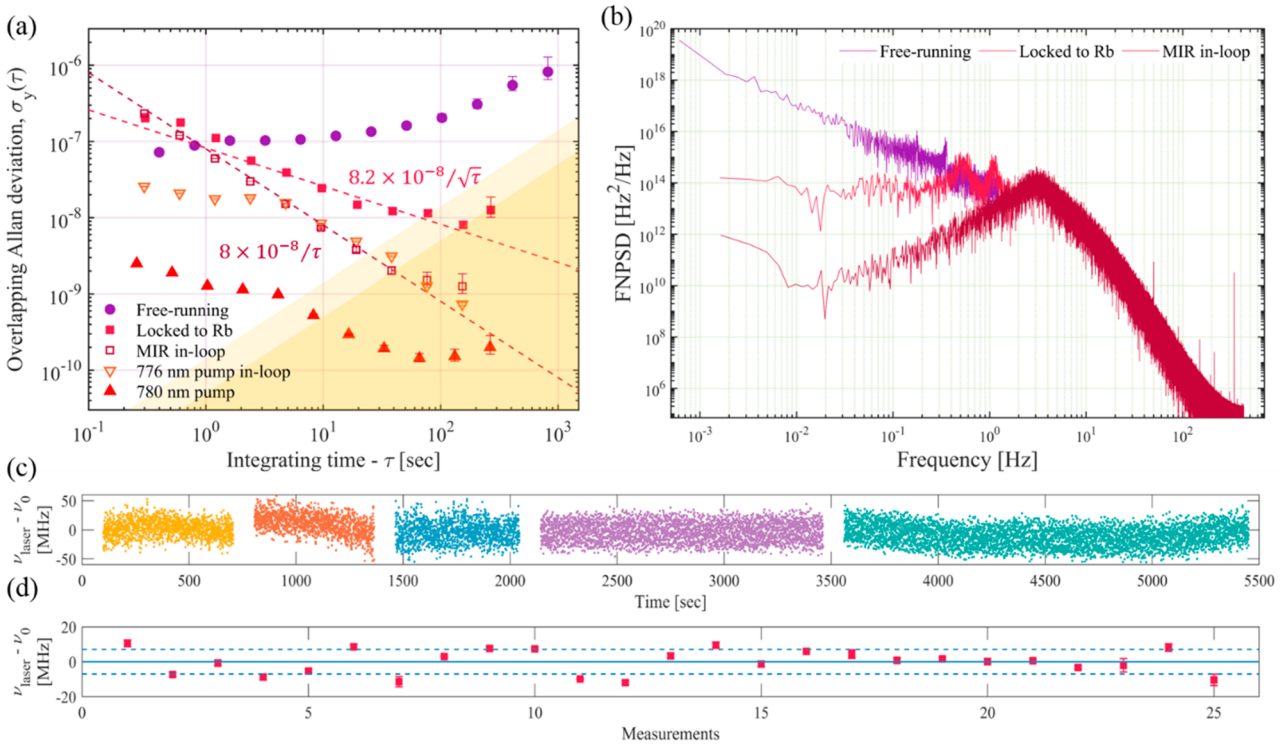

Figure 3. MIR frequency reference precision. (a) The overlapping Allan deviation of the free-running operation (purple circles), and the QCL stabilized to the hyperfine cycling transition of ^{85}Rb (red squares). Error bars represent a 68% confidence interval. Also shown are the major noise sources, including electronic noises and precision of the wavelength meter used in the measurement. The electronic noises are presented as the fractional frequency stability retrieved from the closed-loop servo-electronic signal of the QCL (red open squares) limited by white phase noise, showing a typical of $8 \times 10^{-8}/\tau$. The limit of the wavelength meter is presented by the yellow shaded zone, where the light shaded area represents the estimated limit, according to the manufacturer specification, and the darker one represents its actual limit, based on our measurements. The measured fractional stability of the 780 nm pump, measured by beating it to another 780 nm locked laser (red triangles), and the electronic noise of the 776 nm pump laser (orange open triangles) are also presented for comparison. (b) Measured FNPSD for the free-running regime (purple) and the locked regime (red). We also show the noise of the electronics, which is presented as the FNPSD retrieved from the in-loop error signal. (c) Day to day optical frequency traces obtained by reinitiating the frequency locking to the MIR ^{85}Rb transition. (d) Absolute measurement of the $6^2P_{3/2}(F = 4)-5^2D_{5/2}(F = 5)$ hyperfine transition, extracted from about 25 different measurements. The broken lines highlight the standard deviation from the mean value of ±7 MHz. The error bars of the measurements are smaller than the presented markers.

meter (Figure 3a). The Allan variances, based on this measurement, show a typical white phase noise limited behavior of $8 \times 10^{-8}/\tau$.[40] It should be emphasized that the Allan variance derived from the error signal is relatively insensitive to frequency variations introduced by the discriminator and therefore represents a lower limit of the frequency stability. However, this measurement considers the overall contribution of the shot noise, the electronic noise in the feedback loop, the residual amplitude modulation (RAM) noise that comes from the frequency modulation, and the relative intensity noise (RIN) fluctuations of the lasers at frequencies that produce fictitious error signals after demodulation.

The wavelength-meter adds two types of noises: a white frequency noise and a long-term drift. The white frequency noise is related to its internal electronic noise and from the fluctuations of the position of the laser incident to it. The long-term drift is believed to be associated with its internal frequency reference to which it is calibrated. It has an internal drift related to its locking scheme, and it is sensitive to temperature fluctuations. Our wavelength meter (671B-IR by Bristol Instruments) is calibrated to a standard, nonstabilized, He−Ne laser, presenting a longitudinal mode drift of 0.1 pm, typical of the long-term drift of ±1 MHz in He−Ne lasers.[41]

The output of the wavelength meter was also used for frequency-noise characterization of the QCL. Figure 3b presents the measured frequency-noise power spectral density (FNPSD) in the free-running regime and when the QCL is locked. By closing the frequency-locking loop, the FNPSD is significantly reduced in the low spectral range. A nearly flat FNPSD was measured for the locked case, which is the characteristic of a white frequency noise, attributed to the wavelength meter. The FNPSD obtained from the in-loop error signal shows a typical f^2 behavior in the low frequency range, confirming the hypothesis that the electronic is limited by white phase noise.[40]

Besides the limitations due to our measuring tool, further improvements of the fractional stability of the MIR reference can be obtained by choosing a more advanced locking scheme such as the Pound−Drever−Hall technique, rather than the simple but limited wavelength modulation, at the expense of a substantial increase in complexity and in availability of additional equipment.

In this experiment, the estimated long-term relative stability of the pump lasers was found to be about 1.43×10^{-10} and up to 7.3×10^{-10} for the 780 and 776 nm lasers, respectively. It is interesting to note that, assuming a best-case scenario where the fractional frequency stability of the 776 nm pump laser is

https://dx.doi.org/10.1021/acsphotonics.0c00308
ACS Photonics 2020, 7, 1508−1514

equal to the one measured by in-loop Allan deviation, the 776 nm pump laser frequency stabilization up to 282 kHz is comparable to the 415 kHz of the QCL accuracy. Although there is no clear assessment on the relation between the stability of lasers locked to the same atomic species in a cascaded scheme, a similar correlation was recently reported in experiments involving lasers locked to Rb transitions in a ladder configuration.[42,43]

One of the most important benefits of atomic-Rb stabilization is the long-term repeatability of the frequency stabilization. To assess day-to-day repeatability, we operate the system over a span of about a month. Typical results are presented in Figure 3c, where each of the optical frequency traces (indicated by different colors) represents a frequency measurement performed on a different day. The measured deviation is limited by the repeatability of our wavelength meter. Considering that the system is subjected to environmental perturbations, is unshielded from magnetic fields, and is not packaged, it is very likely that such stability and accuracy can be further improved.

It should be noted that the QCL can be locked to the MIR transition of the Rb not only through the transmission gain spectrum (Figure 2a), but also by using the blue fluorescence enhancement (Figure 2b). In both cases, similar results were obtained. The advantage of using the latter approach is that a conventional silicon photodetector operating in the visible spectral region can be used, rather than using a more advanced MIR photodetector, such as cooled mercury−cadmium−telluride (MCT).

C. Measurement of the $6^2P_{3/2}$−$5^2D_{5/2}$ Transition of ^{85}Rb. Based on the Allan deviation measurement and taking into account the precision and accuracy of our wavelength meter, we have also measured the absolute value of the $6^2P_{3/2}(F = 4)$−$5^2D_{5/2}(F = 5)$ hyperfine transition in ^{85}Rb. Figure 3d shows the data extracted from a large number (ca. 25) of measurements taken over a duration of about a month. The graph also shows the standard deviation limits obtained by fitting the data to a normal distribution. The absolute frequency of the ^{85}Rb transition was found to be 57287162 MHz, with an uncertainty of 7 MHz, limited by our measuring tool. To the best of our knowledge, this is the first time that the absolute frequency of this ^{85}Rb transition in the mid-IR has been measured directly. This transition was measured to be about 27886 MHz, apart from the 1909.9638597 cm^{-1} rovibrational transition of vapor water present in the atmosphere; namely, the (v1, v2, v3, J, Ka, Kc):(0 0 0 6 2 5) → (0 1 0 7 3 4) transition.[44] A wide frequency scan of the MIR QCL presenting these two transitions is presented in Figure 4. The result was obtained by locking the 780 nm and the 776 nm lasers in a counterpropagating mode while scanning the QCL and measuring its transmission through the custom vapor cell.

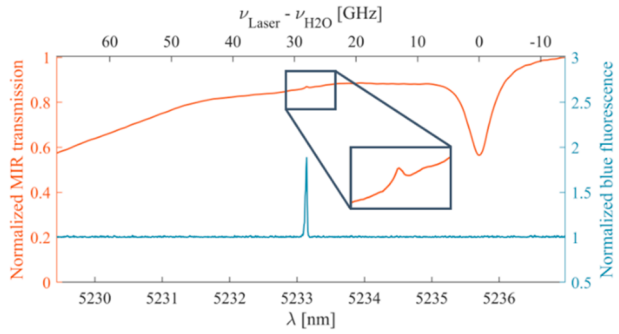

Figure 4. Wide frequency scan around the $6^2P_{3/2}$−$5^2D_{5/2}$ transition of ^{85}Rb, including the (0 0 0 6 2 5) → (0 1 0 7 3 4) transition of water vapor present in the atmosphere. The graph presents the MIR spectroscopy (red) as well as the blue fluorescence of Rb (blue). The inset shows a zoom of the ^{85}Rb MIR transition.

CONCLUSION

In this paper we experimentally demonstrate a method enabling development of frequency standards in the MIR, based on high excited stats of alkali vapors. The technique is based on the generation of a Doppler-free gain spectrum in the MIR, by copropagating two stabilized pump near-infrared (NIR) lasers. Using this technique, we have stabilized the frequency of a distributed feedback (DFB) QCL at 5.23 μm to the corresponding $6^2P_{3/2}$−$5^2D_{5/2}$ transition of Rubidium (Rb) vapors, showing a substantial stability improvement compared to free-running operation. In our experiment, the relative frequency stability and the accuracy of the MIR laser was limited by the accuracy of our measuring tool, presenting an upper limit to the actual frequency stability of the MIR laser. Moreover, the frequency noise characterization indicates that the actual stability of the MIR QCL is limited only by the accuracy of the pump lasers. The frequency stability will be further improved in future experiments. For example, using more advanced locking schemes, a relative stability in the order of 10^{-14} can be achieved for the two pump lasers,[45] simultaneously, and thus, a similar lower limit can be expected in the MIR if one chooses to use a similar scheme.

Stabilization of a laser directly to an atomic mid-infrared transition enables highly accurate molecular spectroscopy in the mid-infrared; either by using a MIR frequency comb stabilized to the presented transition (where one teeth of the frequency comb can be viewed as a CW mid-IR laser) or, alternatively, by using a MIR QCL stabilized to Rb vapors as a highly accurate calibration laser, as part of a self-calibrated highly accurate optical spectrometer.

Furthermore, when the $5^2D_{5/2}$ level of Rb is efficiently populated, simultaneously, population inversion also occurs between the $6^2S_{1/2}$ and $6^2P_{3/2}$ levels of Rb, at a transition wavelength of about 2.73 μm,[46] such that our approach has the potential for stabilizing a MIR frequency comb through nearly an octave, using simultaneously the $6^2S_{1/2}$−$6^2P_{3/2}$ and the $5^2S_{1/2}$−$5^2D_{5/2}$ transitions of Rb, using the same vapor cell. Other wavelengths in the MIR can also be accessed using the presented technique with other alkali atoms.

Finally, the demonstration of frequency stabilization using an atomic MIR transition bares golden opportunities in diverse fields that rely on high precision measurements, including for example sensing, metrology, and free-space communications, to name a few. The establishment of a MIR frequency reference based on alkali vapors and the mature technology gravitating around them could enable applications that require the use of a portable, relatively compact, and highly accurate measuring tools.

ASSOCIATED CONTENT

Supporting Information

The Supporting Information is available free of charge at https://pubs.acs.org/doi/10.1021/acsphotonics.0c00308.

Energy levels of ^{85}Rb and ^{87}Rb; Detailed experimental setup; Theoretical model; Simulation results (PDF)

https://dx.doi.org/10.1021/acsphotonics.0c00308
ACS Photonics 2020, 7, 1508−1514

AUTHOR INFORMATION

Corresponding Author

Uriel Levy − *Department of Applied Physics, the Faculty of Science, the Center for Nanoscience and Nanotechnology, The Hebrew University of Jerusalem, Jerusalem 91904, Israel;* orcid.org/0000-0002-5918-1876; Email: ulevy@mail.huji.ac.il

Authors

Yoel Sebbag − *Department of Applied Physics, the Faculty of Science, the Center for Nanoscience and Nanotechnology, The Hebrew University of Jerusalem, Jerusalem 91904, Israel;* orcid.org/0000-0001-7265-6752

Roy Zektzer − *Department of Applied Physics, the Faculty of Science, the Center for Nanoscience and Nanotechnology, The Hebrew University of Jerusalem, Jerusalem 91904, Israel*

Yefim Barash − *Department of Applied Physics, the Faculty of Science, the Center for Nanoscience and Nanotechnology, The Hebrew University of Jerusalem, Jerusalem 91904, Israel*

Complete contact information is available at: https://pubs.acs.org/10.1021/acsphotonics.0c00308

Funding

The research was supported in part by an ERC Consolidator Grant (LIVIN), by the Israeli Science Foundation (ISF), and by the Israeli Ministry of Science and Technology.

Notes

The authors declare no competing financial interest.

ACKNOWLEDGMENTS

Y.S. acknowledges a fellowship from the center for nanoscience and nanotechnology at the Hebrew University. Y.S. would like to thank Eliran Talker for helpful discussions.

REFERENCES

(1) Ludlow, A. D.; Boyd, M. M.; Ye, J.; Peik, E.; Schmidt, P. O. Optical Atomic Clocks. *Rev. Mod. Phys.* **2015**, *87* (2), 637.

(2) Hinkley, N.; Sherman, A.; Phillips, N. B.; Schioppo, M.; Lemke, N. D.; Beloy, K.; Pizzocaro, M.; Oates, C. W.; Ludlow, A. D. An Atomic Clock with 10−18 Instability. *Science (Washington, DC, U. S.)* **2013**, *341* (6151), 1215−1218.

(3) Oelker, E.; Hutson, R. B.; Kennedy, C. J.; Sonderhouse, L.; Bothwell, T.; Goban, A.; Kedar, D.; Sanner, C.; Robinson, J. M.; Marti, G. E.; et al. Demonstration of 4.8 × 10−17 Stability at 1 s for Two Independent Optical Clocks. *Nat. Photonics* **2019**, *13* (10), 714−719.

(4) Hudson, J. J.; Kara, D. M.; Smallman, I. J.; Sauer, B. E.; Tarbutt, M. R.; Hinds, E. A. Improved Measurement of the Shape of the Electron. *Nature* **2011**, *473* (7348), 493−496.

(5) Tokunaga, S. K.; Stoeffler, C.; Auguste, F.; Shelkovnikov, A.; Daussy, C.; Amy-Klein, A.; Chardonnet, C.; Darquié, B. Probing Weak Force-Induced Parity Violation by High-Resolution Mid-Infrared Molecular Spectroscopy. *Mol. Phys.* **2013**, *111* (14−15), 2363−2373.

(6) Darquié, B.; Stoeffler, C.; Shelkovnikov, A.; Daussy, C.; Amy-Klein, A.; Chardonnet, C.; Zrig, S.; Guy, L.; Crassous, J.; Soulard, P.; et al. Progress toward the First Observation of Parity Violation in Chiral Molecules by High-Resolution Laser Spectroscopy. *Chirality* **2010**, *22*, 870−884.

(7) DeMille, D.; Cahn, S. B.; Murphree, D.; Rahmlow, D. A.; Kozlov, M. G. Using Molecules to Measure Nuclear Spin-Dependent Parity Violation. *Phys. Rev. Lett.* **2008**, *100* (2), 023003.

(8) Daussy, C.; Guinet, M.; Amy-Klein, A.; Djerroud, K.; Hermier, Y.; Briaudeau, S.; Bordé, C. J.; Chardonnet, C. Direct Determination of the Boltzmann Constant by an Optical Method. *Phys. Rev. Lett.* **2007**, *98* (25), 250801.

(9) Hudson, E. R.; Lewandowski, H. J.; Sawyer, B. C.; Ye, J. Cold Molecule Spectroscopy for Constraining the Evolution of the Fine Structure Constant. *Phys. Rev. Lett.* **2006**, *96* (14), 143004.

(10) Jansen, P.; Bethlem, H. L.; Ubachs, W. Perspective: Tipping the Scales: Search for Drifting Constants from Molecular Spectra. *J. Chem. Phys.* **2014**, *140*, 010901.

(11) Knappe, S.; Shah, V.; Schwindt, P. D. D.; Hollberg, L.; Kitching, J.; Liew, L.-A.; Moreland, J. A Microfabricated Atomic Clock. *Appl. Phys. Lett.* **2004**, *85* (9), 1460−1462.

(12) Knabe, K.; Wu, S.; Lim, J.; Tillman, K. A.; Light, P. S.; Couny, F.; Wheeler, N.; Thapa, R.; Jones, A. M.; Nicholson, J. W.; et al. 10 kHz Accuracy of an Optical Frequency Reference Based on 12C_2H_2-Filled Large-Core Kagome Photonic Crystal Fibers. *Opt. Express* **2009**, *17* (18), 16017−16026.

(13) Lurie, A.; Baynes, F. N.; Anstie, J. D.; Light, P. S.; Benabid, F.; Stace, T. M.; Luiten, A. N. High-Performance Iodine Fiber Frequency Standard. *Opt. Lett.* **2011**, *36* (24), 4776−4778.

(14) Newman, Z. L.; Maurice, V.; Drake, T.; Stone, J. R.; Briles, T. C.; Spencer, D. T.; Fredrick, C.; Li, Q.; Westly, D.; Ilic, B. R.; et al. Architecture for the Photonic Integration of an Optical Atomic Clock. *Optica* **2019**, *6* (5), 680.

(15) Hummon, M. T.; Kang, S.; Bopp, D. G.; Li, Q.; Westly, D. A.; Kim, S.; Fredrick, C.; Diddams, S. A.; Srinivasan, K.; Aksyuk, V.; et al. Photonic Chip for Laser Stabilization to an Atomic Vapor with 10−11 Instability. *Optica* **2018**, *5* (4), 443.

(16) Tittel, F. K.; Richter, D.; Fried, A. Mid-Infrared Laser Applications in Spectroscopy. In *Solid-State Mid-Infrared Laser Sources*; Springer Berlin Heidelberg, 2007; pp 458−529.

(17) Schneider, T.; Roth, B.; Duncker, H.; Ernsting, I.; Schiller, S. All-Optical Preparation of Molecular Ions in the Rovibrational Ground State. *Nat. Phys.* **2010**, *6* (4), 275−278.

(18) Bressel, U.; Borodin, A.; Shen, J.; Hansen, M.; Ernsting, I.; Schiller, S. Manipulation of Individual Hyperfine States in Cold Trapped Molecular Ions and Application to HD+ Frequency Metrology. *Phys. Rev. Lett.* **2012**, *108* (18), 183003.

(19) Bressel, U.; Ernsting, I.; Schiller, S. 5 Mm Laser Source for Frequency Metrology Based on Difference Frequency Generation. *Opt. Lett.* **2012**, *37* (5), 918.

(20) Cappelli, F.; Galli, I.; Borri, S.; Giusfredi, G.; Cancio, P.; Mazzotti, D.; Montori, A.; Akikusa, N.; Yamanishi, M.; Bartalini, S.; et al. Subkilohertz Linewidth Room-Temperature Mid-Infrared Quantum Cascade Laser Using a Molecular Sub-Doppler Reference. *Opt. Lett.* **2012**, *37* (23), 4811.

(21) Borri, S.; Galli, I.; Cappelli, F.; Bismuto, A.; Bartalini, S.; Cancio, P.; Giusfredi, G.; Mazzotti, D.; Faist, J.; De Natale, P. Direct Link of a Mid-Infrared QCL to a Frequency Comb by Optical Injection. *Opt. Lett.* **2012**, *37* (6), 1011.

(22) Galli, I.; Siciliani De Cumis, M.; Cappelli, F.; Bartalini, S.; Mazzotti, D.; Borri, S.; Montori, A.; Akikusa, N.; Yamanishi, M.; Giusfredi, G.; et al. Comb-Assisted Subkilohertz Linewidth Quantum Cascade Laser for High-Precision Mid-Infrared Spectroscopy. *Appl. Phys. Lett.* **2013**, *102* (12), 121117.

(23) Sow, P. L. T.; Mejri, S.; Tokunaga, S. K.; Lopez, O.; Goncharov, A.; Argence, B.; Chardonnet, C.; Amy-Klein, A.; Daussy, C.; Darquié, B. A Widely Tunable 10 Mm Quantum Cascade Laser Phase-Locked to a State-of-the-Art Mid-Infrared Reference for Precision Molecular Spectroscopy. *Appl. Phys. Lett.* **2014**, *104* (26), 264101.

(24) Argence, B.; Chanteau, B.; Lopez, O.; Nicolodi, D.; Abgrall, M.; Chardonnet, C.; Daussy, C.; Darquié, B.; Le Coq, Y.; Amy-Klein, A. Quantum Cascade Laser Frequency Stabilization at the Sub-Hz Level. *Nat. Photonics* **2015**, *9* (7), 456−460.

(25) Bernard, V.; Daussy, C.; Nogues, G.; Constantin, L.; Durand, P. E.; Amy-Klein, A.; Van Lerberghe, A.; Chardonnet, C. CO2 Laser Stabilization to 0.1 Hz Level Using External Electrooptic Modulation. *IEEE J. Quantum Electron.* **1997**, *33* (8), 1282−1287.

(26) Acef, O. Metrological Properties of CO2/OsO4 Optical Frequency Standard. *Opt. Commun.* **1997**, *134* (1−6), 479−486.
(27) Amy-Klein, A.; Vigué, H.; Chardonnet, C. Absolute Frequency Measurement of 12C16O2 Laser Lines with a Femtosecond Laser Comb and New Determination of the 12C16O2Molecular Constants and Frequency Grid. *J. Mol. Spectrosc.* **2004**, *228* (1), 206−212.
(28) Bartalini, S.; Cancio, P.; Giusfredi, G.; Mazzotti, D.; De Natale, P.; Borri, S.; Galli, I.; Leveque, T.; Gianfrani, L. Frequency-Comb-Referenced Quantum-Cascade Laser at 4.4 Mm. *Opt. Lett.* **2007**, *32* (8), 988.
(29) Gatti, D.; Gambetta, A.; Castrillo, A.; Galzerano, G.; Laporta, P.; Gianfrani, L.; Marangoni, M. High-Precision Molecular Interrogation by Direct Referencing of a Quantum-Cascade-Laser to a near-Infrared Frequency Comb. *Opt. Express* **2011**, *19* (18), 17520.
(30) Mills, A. A.; Gatti, D.; Jiang, J.; Mohr, C.; Mefford, W.; Gianfrani, L.; Fermann, M.; Hartl, I.; Marangoni, M. Coherent Phase Lock of a 9 Mm Quantum Cascade Laser to a 2 Mm Thulium Optical Frequency Comb. *Opt. Lett.* **2012**, *37* (19), 4083.
(31) Chanteau, B.; Lopez, O.; Zhang, W.; Nicolodi, D.; Argence, B.; Auguste, F.; Abgrall, M.; Chardonnet, C.; Santarelli, G.; Darquié, B.; et al. Mid-Infrared Laser Phase-Locking to a Remote near-Infrared Frequency Reference for High-Precision Molecular Spectroscopy. *New J. Phys.* **2013**, *15*, 073003.
(32) Sakai, Y.; Yokohama, I.; Kominato, T.; Sudo, S. Frequency Stabilization of Laser Diode Using a Frequency-Locked Ring Resonator to Acetylene Gas Absorption Lines. *IEEE Photonics Technol. Lett.* **1991**, *3* (10), 868−870.
(33) Kitching, J. Chip-Scale Atomic Devices. *Appl. Phys. Rev.* **2018**, *5*, 031302.
(34) Akulshin, A.; Budker, D.; McLean, R. Directional Infrared Emission Resulting from Cascade Population Inversion and Four-Wave Mixing in Rb Vapor. *Opt. Lett.* **2014**, *39* (4), 845−848.
(35) Akulshin, A. M.; Rahaman, N.; Suslov, S. A.; McLean, R. J. Amplified Spontaneous Emission at 5.23 Um in Two-Photon Excited Rb Vapour. *J. Opt. Soc. Am. B* **2017**, *34* (12), 2478.
(36) Sebbag, Y.; Barash, Y.; Levy, U. Generation of Coherent Mid-IR Light by Parametric Four-Wave Mixing in Alkali Vapor. *Opt. Lett.* **2019**, *44* (4), 971.
(37) Antypas, D.; Tretiak, O.; Budker, D.; Akulshin, A. Polychromatic, Continuous-Wave Mirrorless Lasing from Monochromatic Pumping of Cesium Vapor. *Opt. Lett.* **2019**, *44* (15), 3657.
(38) Supplee, J. M.; Whittaker, E. A.; Lenth, W. Theoretical Description of Frequency Modulation and Wavelength Modulation Spectroscopy. *Appl. Opt.* **1994**, *33* (27), 6294.
(39) Safronova, M. S.; Williams, C. J.; Clark, C. W. Relativistic Many-Body Calculations of Electric-Dipole Matrix Elements, Lifetimes, and Polarizabilities in Rubidium. *Phys. Rev. A: At., Mol., Opt. Phys.* **2004**, *69* (2), 022509.
(40) Rubiola, E. *Phase Noise and Frequency Stability in Oscillators*; Cambridge University Press, 2008.
(41) Wallard, A. J. Frequency Stabilization of the Helium-Neon Laser by Saturated Absorption in Iodine Vapour. *J. Phys. E: Sci. Instrum.* **1972**, *5* (9), 926−930.
(42) Lee, W.-K.; Seb Moon, H.; Suhng Suh, H. Measurement of the Absolute Energy Level and Hyperfine Structure of the 87Rb 4D5/2 State. *Opt. Lett.* **2007**, *32* (19), 2810.
(43) Stern, L.; Stone, J. R.; Kang, S.; Cole, D. C.; Suh, M. G.; Fredrick, C.; Newman, Z.; Vahala, K.; Kitching, J.; Diddams, S. A.; et al. Direct Kerr Frequency Comb Atomic Spectroscopy and Stabilization. *Sci. Adv.* **2020**, *6* (9), No. eaax6230.
(44) Birk, M.; Wagner, G.; Loos, J.; Lodi, L.; Polyansky, O. L.; Kyuberis, A. A.; Zobov, N. F.; Tennyson, J. Accurate Line Intensities for Water Transitions in the Infrared: Comparison of Theory and Experiment. *J. Quant. Spectrosc. Radiat. Transfer* **2017**, *203*, 88.
(45) Perrella, C.; Light, P. S.; Anstie, J. D.; Baynes, F. N.; White, R. T.; Luiten, A. N. Dichroic Two-Photon Rubidium Frequency Standard. *Phys. Rev. Appl.* **2019**, *12* (5), 054063.
(46) Moran, P. J.; Richards, R. M.; Rice, C. A.; Perram, G. P. Near Infrared Rubidium 62P3/2,1/2−62S1/2 Laser. *Opt. Commun.* **2016**, *374*, 51−57.

https://dx.doi.org/10.1021/acsphotonics.0c00308
ACS Photonics 2020, 7, 1508−1514